Al-Khwarizmi Engineering Journal
ISSN (printed): 1818 – 1171, ISSN (online): 2312 – 0789
Vol. 20, No. 4, December (2024), pp. 58-69

Al-Khwarizmi Engineering Journal

# Modified Study for the Effect of Combined Cycling Loading in Plane on Dynamic Edge Crack Propagation in a Thin Plate

**Israa Abed Alrazak Mosleh[1*], Fathi A. A. Alshamma[2]**
[1,2] *Mechanical Department, College of Engineering, University of Baghdad, Baghdad, Iraq*
*Corresponding Author's Email: israa.mosleh2003m@coeng.uobaghdad.edu.iq

(Received 11 September 2023; Revised 26 December 2023; Accepted 19 March 2024; Published 1 December 2024)
https://doi.org/10.22153/kej.2024.03.003

## Abstract

The significant risks associated with the occurrence of mechanical cracks in engineering applications are investigated in this paper. In particular, the specific type of crack propagation that results from mixed mode loading (modes I and II), which spreads throughout most structures, and the conditions under which it can occur are presented. Following the linear elastic fracture mechanics theory, non-proportional loading on specimens of aluminium alloy was accomplished by applying constant tensile loads in conjunction with periodic shear loads. A theoretical equation for the dynamic crack growth rate was constructed using Griffiths law for mixed mode I/II of the dynamic crack growth. This equation considers the influence of dynamic crack propagation. Experimentally, a locally designed laboratory apparatus was modified to suit the nature of the applied loads on samples with edge pre-cracks and two types of samples of aluminium alloys (AA), 6061 and 5052, at the Uni-Standard System with an edge crack length of 5 mm at mid were used. A comparison of the types of alloys used to verify the validity of the results was performed. The results showed acceptable agreement in determining crack propagation rate when predicting the results of the theoretical and experimental analyses. The results in the sample showed 5052 (0.0006, 0.000633) mm/sec for the experimental and theoretical results, respectively. In contrast, the crack propagation rate amounted to 6061 (0.000183, 0.000222) mm/sec for the experimental and theoretical results, respectively. Hence, Sample 5052 started faster and propagated cracks faster than alloy 6061.

***Keywords:*** *mixed mode; shear cycling load; crack propagation; combined loads and crack growth*

## 1. Introduction

Mechanical fracture is one of the problem types of failure that must be considered when analysing and constructing any structural or mechanical machine because crack growth is one of the most common causes of failure in material [1][2]. Hence, investigating the types of mechanical failures that can happen and represent a risk to human lives and material losses is necessary to treat or prevent occurences. The majority of mechanical applications, including to bridges, aircraft, and shafts that conduct movement, are subjected to compound loads. These combined loads are subdivided into proportional and non-proportional loads. Detecting the highest stress or calculating the magnitude of non-proportional loading in mechanical construction can be very challenging. Moreover, pinpointing exactly where the collapse will occur is impossible. The timing of the first crack propagation and the pace at which the crack spreads are the two primary factors considered when determining how long a mechanical fracture will last. Many factors are affected by cracks resulting from the mixed mode [3]____ that affect it directly. Moreover, the ratio of the length of the crack should not exceed stage I; that is, it should remain within the first stage in the Paris Eq. (1).

$$\left((da/dN) = C(\Delta k_{equ})^{m}\right) \quad \ldots(1)$$

where the K equivalent represents the value of the equivalent stress intensity factor for Modes I and II, which represents the difference between the maximum and minimum values of the equivalent

stress intensity factor. A number of factors, which have a direct effect on the growth and velocity of spread include the rate of diffusion, age of the metal, nanostructure of the metal[4], [5] and temperature [6], [7] shoud also be considered to avoid propagation in the material. Jahed and Col suggested using the formulas model, which focuses on the strain energy of the various metals. The occurrence of failure on various metallic materials can be anticipated by applying uniaxial and proportional loading at low cycle fatigue and high cycle fatigue. The complete failure of the material is based on the sum of their strain energies when it is in the condition of elasticity and plasticity. This approach can be achieved by applying loading in both the longitudinal and transverse directions [8]. Zain and Alshamma designed a new laboratory apparatus capable of applying single or multiple cyclic loadings, which facilitated the analysis of samples of genuine tubes with realistic sizes and the study of crack growth rate experimentally and numerically using the Forman equation [9]. Salman studied the effects of laser strikes on the formation of cracks in metals using a wide range of aluminium alloys (7049, 7050, 2024, and 6061) with thicknesses of 1 mm and 2 mm. The study used a laser cutting machine to create a central crack, and a Neodymium-doped Yttrium Aluminum Garnet laser to harden the area around the crack [10]. Wang et al. investigated the dynamic crack growth on glass samples filled with epoxy with varied lengths of cracks, and the spreading rate and effect of these lengths on enhancing the spreading rate in the mixed mode of loading [11].

Two types of methods are generally used in treating the occurrence of cracks in the mechanical structure. The first type of method is treatment methods. such as welding, heat treatment, etc., which may not be effective in preventing the growth of the crack or may be expensive. The second type of method lies in predicting the rate of propagation speed in the material, which is possible by studying the rates of the possibility of failure occurring in the material. This is the subject of study in this research, which deals with two different types of aluminium alloys [12] selected for the purpose of conducting fracture and crack growth tests. These aluminium alloys can be specified under UNI Standard 5052 and 6061 [13] based on hardening Vickers tests [14] and chemical composition analysis [15]. The tests were conducted to determine the type of specification within the temperature range of 27 °C and humidity of 20%.

The main objectives of this research are as follows:

- Study the crack growth rate and predict the instability stage entering to avoid failure in the material.
- Design an apparatus that applies combined fatigue loads to specimens by applying a constant tensile load and cyclic shear loads.
- Identify the crack initiation and propagation rates for two types of aluminium alloys and comparing their results and behaviours.
- Derive an equation for finding the crack growth rate using the Griffith energy balancing method and verify the experimental result.

## 2. Methods

### 2.1 Theoretical Analysis

When studying a thin plate that is subjected to two different kinds of loads, such as in-plane, constant tensile load ,and on the other axis of cycling shear loading, in the theoretical calculations, the material is assumed to be linearly elastic calculation, follows Hooke's law, is isotropic and homogeneous. It is very important to derive an analytical model that can predict the occurrence of cracks and their propagation over a number of cycles. The crack growth rate for the mixed mode I/II was extracted using equations, and an equation was derived using the Griffith energies balancing equation for dynamic crack growth. The principle behind this equation is that the ratio of the perpendicular displacement to the direction of stress for both axes at the mixed mode I/II loading in-plane is extracted and the energy result used to drive the crack growth equation.

#### 2.1.1 Analytical model of displacement

The Westergaard stress function is used to analyse crack propagation in mixed mode [16].

$$\boldsymbol{\phi}_{Z(I+II)} = \frac{\sigma . Z}{\sqrt{Z^2 - a^2}} \quad \ldots(2)$$

The following relationships can be derived from Equation (1):

$$z = r.\, e^{i\boldsymbol{\theta}} \quad \ldots(3)$$

$$z\text{-}a = r_1 .e^{i\boldsymbol{\theta}_1} \quad \ldots(4)$$

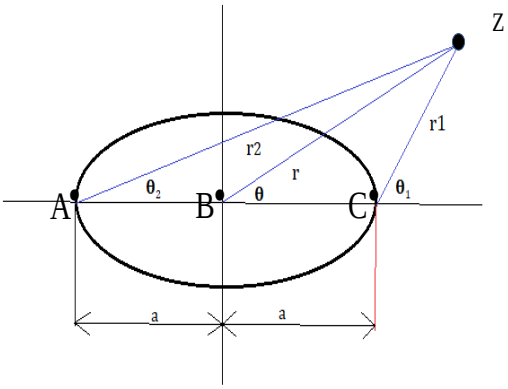


**Fig. 1. Standing theory of cracks. The Westergaard equation based on [17] is used to solve the complex number using the Airy stress function.**

$$z + a = r_2 . e^{i\theta_2} \quad \ldots(5)$$

where z is a complex function with the variable position located on the plate found relative to the points on cracks A, B and C [17].

For plain strain:

$$V = \frac{2\sigma_{eff}}{E}(1-\upsilon^2).\sqrt{a^2-x^2}.$$

For plain stress:

$$V = \frac{2\sigma_{eff}}{E\prime}.\sqrt{a^2-x^2} \quad \ldots(6)$$

where $\frac{1}{E\prime} = \frac{(1-\upsilon^2)}{E}$, assume $x = ca \quad 0 < x < 1$, let $c_1 = 2\sqrt{1-c^2}$, based on that, the displacement of the crack (V) for the mixed mode I/II is

$$V = \frac{c_1}{E}.\sigma_{eff}.a \quad \ldots(7)$$

The effective stress $\boldsymbol{\sigma}_{eff}$ for mixed mode I/II comes from the tensile load in direction and cycling shear load within the elastic limit in MPa [18], as shown in Fig. 2.

$$\sigma_{eff} = \frac{1}{\sqrt{2}}\sqrt{[\sigma^2 + (\tau_o.\sin\left(\frac{w.t}{2}\right))^2]} \quad \ldots(8)$$

The rate of displacement ($\dot{V}$) is determined by subtracting Equation (8) from Equation (7) and then constructing the equation for the stress and crack length variables using this information.

$$\dot{V} = \frac{c_1}{E`}.[\frac{a_o}{\sqrt{2}}.\frac{w.\tau_o^2.\sin(w.t)}{4\left[\sigma^2 + \left(\tau_o.\sin\left(\frac{w.t}{2}\right)\right)^2\right]^{1/2}} + \frac{1}{\sqrt{2}}.\left[\sigma^2 + \left(\tau_o.\sin\left(\frac{w.t}{2}\right)\right)^2\right]^{1/2}.\frac{da}{dt}] \quad \ldots(9)$$

To determine the entire amount of kinetic energy [19], denoted as ($T_{total}$),

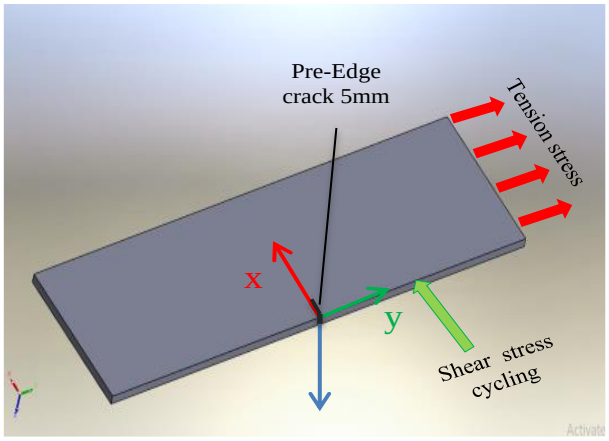


**Fig. 2. Loads on the sample, which shows the method of exposing fatigue loads on the plate in the device (constant tensile stress towards the Y-axis and periodic shear loads by pressing the sample parallel to the X-axis within the elastic limit ) to obtain the type of non-proportional loads with mixed mode.**

$$= \frac{1}{2}.\rho.\text{area}.v^{\bullet 2} \quad \ldots(10)$$

After making substitutions in Eqs. (8–10) and deriving the displacement of the crack (V) and the stresses, the total kinetic energy ($T_{total}$) equation was obtained as follows:

$$T_{total} = \frac{\rho\, k a_i^2}{2E^{\prime 2}}[\left(\sigma^2 + \tau^2 \sin^2\left(\frac{w.t}{2}\right)\right).\left(\frac{da}{dt}\right)^2 + \tau^2.a_o\frac{w}{2}.\sin\left(\frac{w.t}{2}\right).\left(\frac{da}{dt}\right) + \tau_o^2.a_o^2\frac{w^2}{4}.cos^2\left(\frac{w.t}{2}\right)] \quad \ldots(11)$$

### 2.1.2. Excess energy rate

To determine the excess energy rate (U) controlled by the crack's extension at the mixed modes (I/II) in the thin plate [17], [18] for Fig. 3, the following equation is used:

$$U = \int_{a_o}^{a_i}(G-R).da = -\int_{a_o}^{a_i} R.da + \int_{a_o}^{a_i} G.da \quad \ldots(12)$$

The total excess energy (U) for the mixed modes I/II [5], [20] is determined as follows:

$$U = \left(\frac{\sigma^2}{2E} + \frac{2(1+\upsilon)}{E}\left(\tau_o.\sin\frac{wt}{2}\right)^2\right) \quad \ldots(13)$$

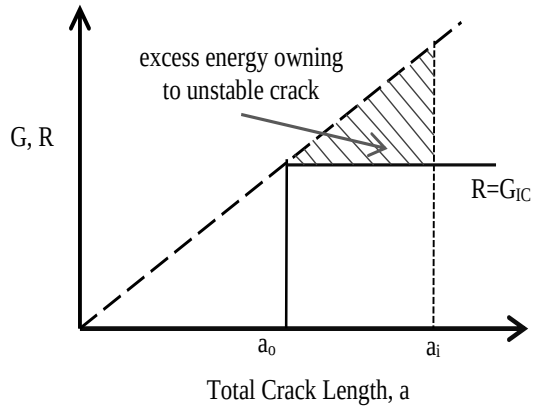


**Fig. 3. Energy balance of the crack, which demonstrates the effect of the balance of energies and the influence that the amount of excess energy exerted on the plate in terms of the increase in the crack length from ($a_o$) to ($a_i$)** [17].

Physically, it has been scientifically proven [21], [22] that the deformation that appears at the crack edge, which forms the plastic area around and at the tip of the crack, enhances the resistance to the appearance of cracks. As a result, the necessary energy that the crack needs to start growing is higher in the crack at the middle because of the two tips of the crack in the centre crack in the plate.

Therefore, this research adopts the assumption adopted that the energy surrounded by the crack is defined as an area that resembles a circle. The excess energy required to start the growth of the crack is less in the case of the crack at the edge (that is, it requires less energy to appear to grow). The excess energy is expressed in the speed of the risk of spread rate and the size of the circle surrounding the crack is not similar in the previously studied cases. The area is smaller, and the diameter of the circle becomes (a), as shown in Fig. 4, and the radius of the circle is (a/2), where the prediction of the theoretical results will be compared later with the propagation rate of the crack and its failure to reach the stage of failure, the experimental results.

The amount of excess energy, $U_o$, per unit thickness for an edge crack is as follows:

$$U_O = \left(\frac{\sigma^2}{2E} + \frac{2(1+\upsilon)}{E}\left(\tau_o . \sin\frac{wt}{2}\right)^2\right).\frac{\pi a^2}{4} \quad \ldots(14)$$

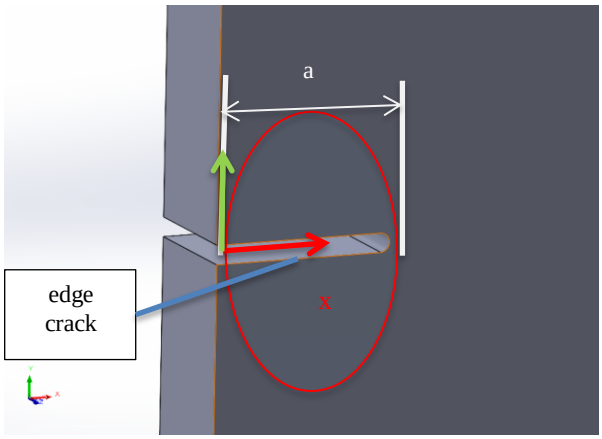


**Fig. 4. Energy around the crack at the edge of the sample.**

The value of the excess energy is transformed into the total energy as the cracking begins to propagate. This conversion results in kinetic energy and heat; however, the heat energy is negligible in a thin plate and can be ignored ($U = T_{Total}$).

$$\left(\frac{\sigma^2}{2E} + \frac{2(1+\upsilon)}{E}\left(\tau_o . \sin\frac{wt}{2}\right)^2\right)\frac{\pi a^2}{4} =$$
$$\frac{\rho\, k a_i^2}{2E^2}\left[\left(\sigma^2 + {\tau_o}^2 \sin^2\left(\frac{wt}{2}\right)\right).\left(\frac{da}{dt}\right)^2\right.$$
$$+{\tau_o}^2 . a_o . \frac{w}{2} . \sin\left(\frac{wt}{2}\right).\left(\frac{da}{dt}\right)$$
$$\left.+{\tau_o}^2 . a_o^2 \frac{w^2}{4} . \cos^2\left(\frac{wt}{2}\right)\right] \quad \ldots(15)$$

where Equation (15) is the final crack growth equation.

## 3. Experimental Work

Before the samples undergo the apparatus, the mechanical properties, which are represented by conducting the Vickers hardness test and the tensile test, and the chemical properties, must be determined.

The X-ray device was used to analyse the samples to study and understand their properties, components of chemical elements, and engineering behaviour as shown in Fig. 5.

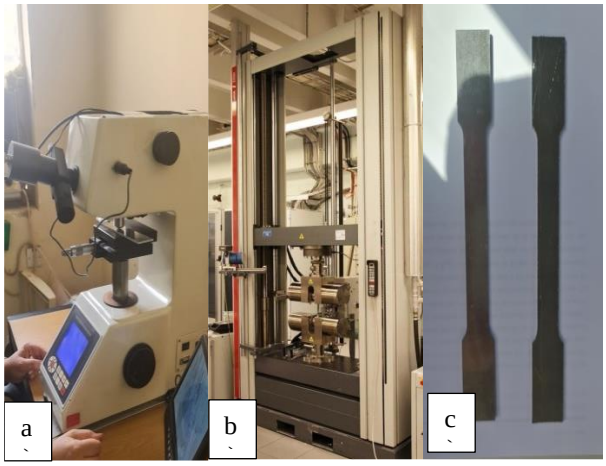


**Fig. 5. Mechanical tests: a) Vickers hardening test; b) Zwick tensile test machine; c) Standard specimens for tensile test.**

Tables 1 and 2 show the chemical composition and mechanical properties of the samples.

**Table 1,**
**Chemical composition for samples**

| Elements | 6061 AA | 5052AA |
|---|---|---|
| Si | 0.34 | 0.491 |
| Fe | 0.514 | 0.491 |
| Cu | 0.043 | 0.249 |
| Mn | 0.118 | 0.0988 |
| Mg | 2.59 | 0.933 |
| Cr | 0.0168 | 0.108 |
| Ni | 0.0063 | 0.0076 |
| Zn | 0.0376 | 0.0242 |
| Ti | 0.008 | 0.0093 |
| Pb | 0.0156 | 0.012 |
| Al | 96.3 | 97.6 |

**Table 2,**
**Mechanical properties for samples**

| properties | 6061 AA | 5052 AA |
|---|---|---|
| Ultimate stress (MPa) | 288.95 | 215.34 |
| Yield stress (MPa) | 249.65 | 106.23 |
| Elongation % | 13.8 | 106.23 |
| Hardening | 98 | 60 |
| Vickers test modules of Elasticity (Gpa) | 68.9 | 70.3 |

The research apparatus that applies a combined load on the sample was designed regionally [5]. The tensile load is applied in the vertical direction relative to the level of the crack surface to generate the opening mode (mode I), and the apparatus is placed on the other axis of the specimen to be the cycling load to develop into mode II, which consists of periodic shear loading. The apparatus generates both modes. A hydraulic system includes a hydraulic pump, hydraulic transmission tube, pressure gauge to indicate the amount of tension applied to the sample and manual lever to operate the hydraulic pump that produces the tension force. In terms of cycling shear stress, the movement is produced by an electric motor with a rotational speed of 1000 revolutions per minute in direct current type with three phases. It transmits a shaft through a V-type transmission belt and a lever connected to the shaft is used to convert it into a linear motion. This is the location where the rotational motion is transformed into a linear motion. Figs. 7 and 8 show the lever possesses a screw for the purpose of controlling the amount of displacement that enters the sample holder.


**Fig. 6: a) Strain meter device; b) Strain gauge paste on the specimen.**

This step allows the value of the shear strain that was applied on the specimen to be measured by two strain gauges with 120 ohms attached at the centre of the sample and to the top and bottom faces (half-bridge) [24], see Fig. 6 (a and b).

Six sample clamps make up the total number available; two are permanently attached, and the fourth clamp is fixed.

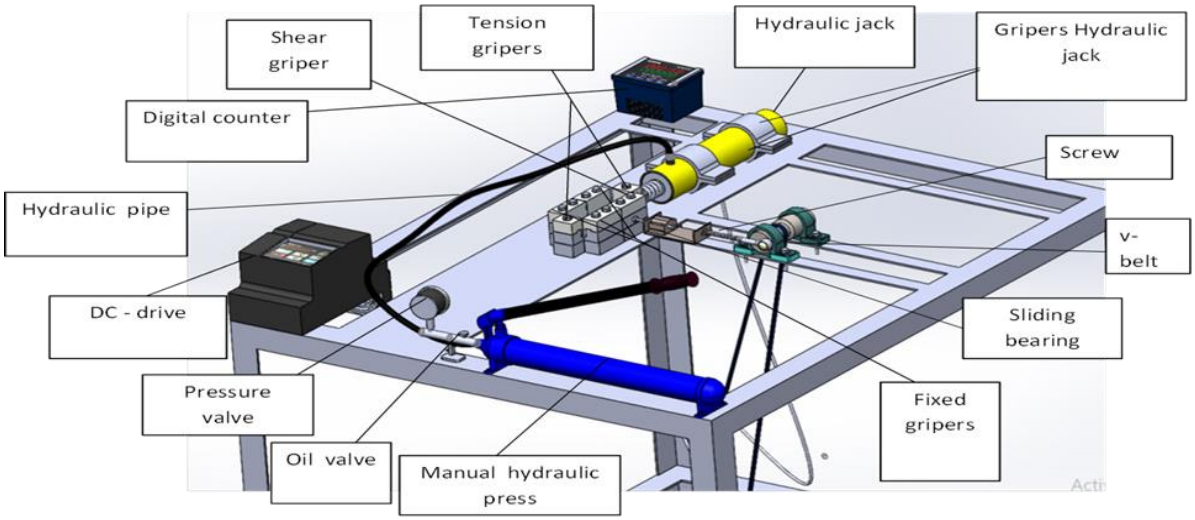


**Fig. 7. Section of the Device by Solid Work Program**

One of the movable sample grippers is connected to the hydraulic pump that pulls it out with a tensile strength of 30 bar. The other gripper is connected to the arm generating periodic shear load on the sample with an entry value of 0.00188 of shear strain to ensure that the stresses investigated under the high fatigue cycle theory are within the elastic limit. Fixed tensile stress was applied to the y-axis while cyclic shear stress with its lowest value equal to zero and its highest value equal to ($\tau$ = 49.088 MPa) was applied to the x-axis.

**Fig. 8. Section of the fatigue device**

The specimen has an edge pre-crack length of 5 mm and a thickness of 0.2 mm; the overall dimensions of the specimen are 160 x 40 x 2mm. The specimen was cut and cracked using a wire-cutting (electrical discharge machining), as shown in ( Fig. 9).

a)

b)

**Fig. 9: a) Aluminium alloy specimen b) Crack propagation**

The growth of the crack in the sample was observed using a digital camera (Nikon Coolpix B700), and the data were transformed to determine the length of the crack using the image processing software (IMAGE J).

## 4. Results and Discussion

The results of the experiments indicate differences in the rate of crack initiation and growth between the 6061 and 5052 aluminium alloys. The differences were based on the elasticity of the material, which is the initiation of life, and the crack

growth rate will decrease as this rate increases. In contrast, if initiation does not occur, the growth rate will rise, and the material will be characterised as brittle.

The results of the rate of crack length during the time and number of cycles N were compared with the data generated from the theoretical analysis equation derived in study (Equation (15)).

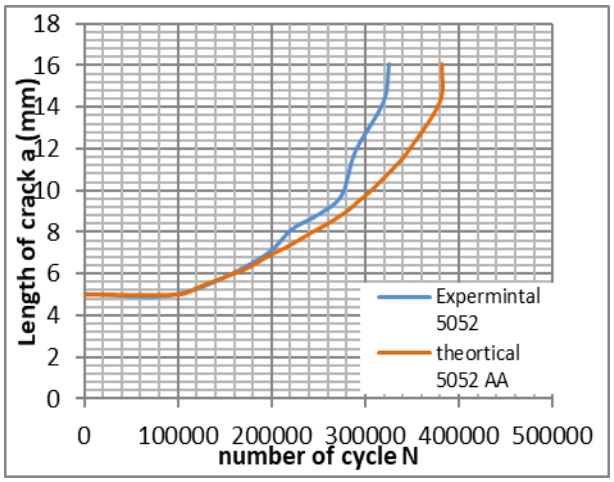


**Fig. 10. Result of (a-N) for alloy 5052.**

A comparison of the number of cycles (N) with the length of the crack (a) formed for the experimental and theoretical results from (Equation 15) for sample 5052, in which the pre-prepared crack begins to grow at 100,000 cycles shows that initially, the results are close, reaching a length of 7 mm 195,000 cycles. At a length of 14 mm, the crack begins to increase in growth velocity, indicating that it has reached the instability stage. Fig. 10 shows that the general crack growth rates were 0.0006 and 0.000633) mm/s for the experimental and theoretical results from (Equation 15).

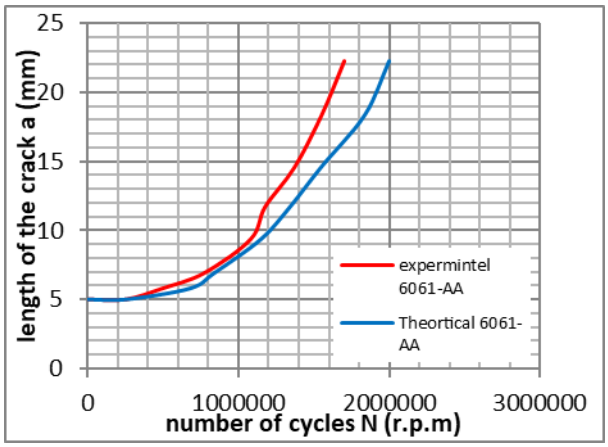


**Fig. 11. Results in (a-N) for alloy 6061.**

For sample 6061, the number of cycles (N) and the length of the crack (a) formed for the experimental and theoretical results from Equation 15 where the crack of initiation was at 250000 cycles. The results are close, and the length of 10 mm was reached when the number of cycles of 1075,000 cycles. Figure 11 shows that at the length of 18 mm, the crack begins to increase in the growth velocity, indicating that it has entered the instability stage. The general crack growth rates were (0.000183 and 0.000222 mm/s for the experimental and theoretical results from (Equation 15).

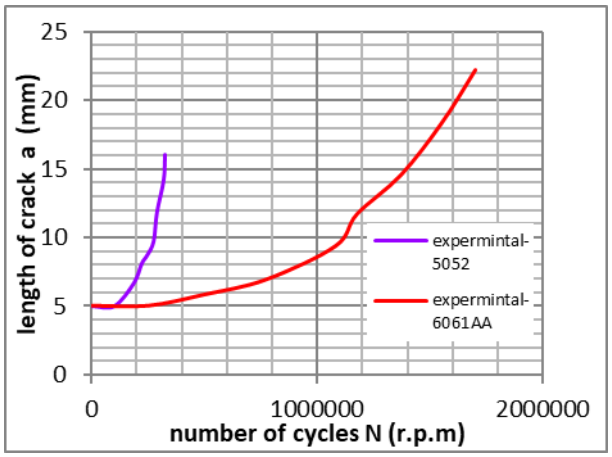


**Fig. 12. Experimental results of (a-N) for alloys 6061 and 5052.**

The m and C values of the Paris equation [25] were extracted experimentally and analytically using the log plot method, where the value of C is ($8.5113*10^{-7}$, $6.309*10^{-7}$) $(\text{mm/cycle})/(MPa\sqrt{m})$ and m is (2.3571, 2.428) for alloy 6061, while the value of C is ($2.958*10^{-6}$, $4.6773*10^{-6}$) $(\text{mm/cycle})/(MPa\sqrt{m})$ and m is (2.056, 1.6609) for alloy 5052.

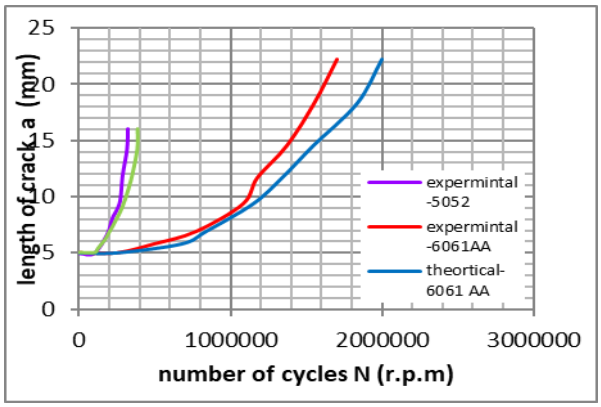


**Fig. 13. Experimental and theoretical results for the alloy**

The crack initiation for the two samples at 100,000 and 250,000 cycles for the two samples, 5052 and 6061 were based on the experimental results as shown in Figs. (10–13).

In contrast to the crack that occurred in sample 6061, which could be difficult to observe with the naked eye because of the molecular characteristics of the material, the shape of the crack in sample 5052–AA was often plainly apparent and contains simple granular zigzags.


**Fig. 14. Crack propagation in alloys experimentally: a. alloy 5052-AA; b. alloy 6061-AA**

In contrast, the crack that formed in sample 6061 was difficult to notice with the naked eye, as shown in Fig. 14. Initially, an agreement in the prediction of the findings could be observed and used to examine the relation between the length of the crack and the number of cycles. When the results are compared with the analysis using the mathematical model delivered to fit into the mixed mode I/II non-proportional loading applied on the sample, Figs. 15 and 16 show the stages of crack growth in the samples

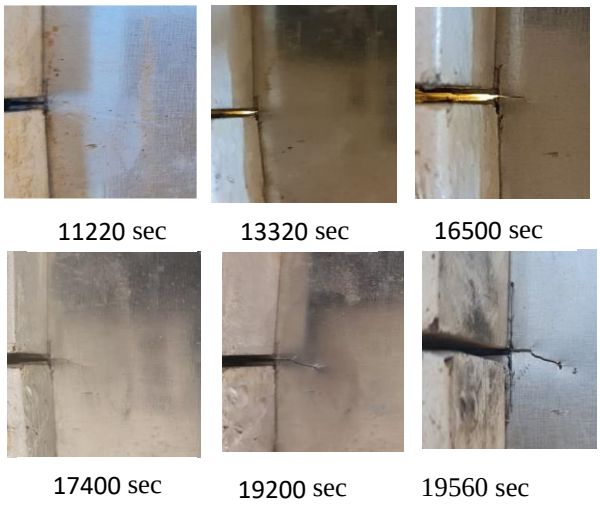


**Fig. 15. Crack growth steps in 5052-AA.**

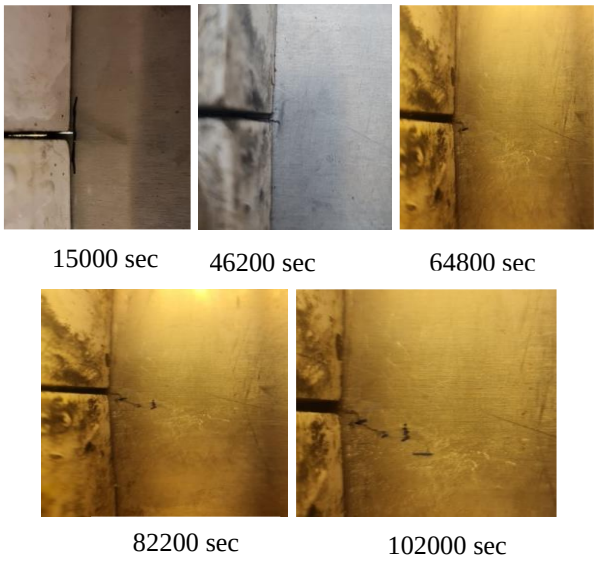


**Fig. 16. Crack growth steps in 6061-AA.**

When the number of cycles is increased, a difference can be observed between the experimental and theoretical curves. The reason for this difference is due to the nature of the material [26] in the experimental test; the material used was a commercial material intended to examine normal behaviour when cracking occurs in the structures and mechanical parts. It is not a standard alloy (because of the presence of impurities and the granular structure of the material). Moreover, despite the vibration being basic [23], it can influence the spread because it is created by the device when it rotates at a high speed and the test temperature.

## 5. Conclusion

- The experimental results are consistent with the mathematical model developed for the research. The estimate of a crack growing in the material at the beginning of the chart indicates the connection between the length of the fracture and the number of cycles.
- It was shown from the procedures of studying experimental fatigue test methods for cyclic loads on materials that the initiation of crack for sample 6061 was larger than that for sample 5052 by a percentage equal to 60%.
- The experimental work shows the rate of crack growth in sample 6061 AA was lower than the rate of crack growth in sample 5052 AA. This finding implies that sample 6061 requires more time than sample 5052 to reach the failure stage,

also known as mechanical fracture, with a percentage of 75.03%.

- Based on the composition of the chemical properties of the samples and the rate of crack growth, it can be inferred that the samples within aluminium alloy 6061 are ductile material alloys with relatively small grain size. This characteristic explains why the rate of crack growth in that type of alloy is slow; the small grains increase the possibility of crack occurrence, which, in turn, causes the rate of crack growth to become slower. A relatively plastic strain between the grains, in addition to the production of big plastic deformation in the area surrounding the fracture in an attempt to prevent the crack from happening and for the same reason, may explain why this would be the case.
- In contrast to sample 5052, which is defined by big grains, the speed of spread of the crack and the great distance to the crack that grew, this sample is distinguished by the type and shape of the crack that formed within it, which is specified as a brittle material.
- Some influencing variables, in addition to the basic nature of the alloy's elemental makeup, are responsible for the difference that may be observed between the experimental and theoretical results at the end of the crack formation process.
- A comparison of the analytical findings for alloy 5052 with the experimental result indicated the analytical model with the error rate in crack growth rate is 5.23%. The percentage of error for alloy 6061 is 17.5%, which is a good estimate for estimating the time of failure.
- The C and m values found for the Paris relation crack propagation through the application of the logarithmic diagram are at acceptable levels within the ranges that aluminium alloys have defined for themselves.

**Nomenclature and Units**

| | |
|---|---|
| da/dN | Fatigue crack growth rate, mm / cycle |
| $K_{eq}$ | Stress intensity factor equivalent, Mega Pascal. |
| m | Constant factor of Paris equation, unitless. |
| C | Constant factor of Paris equation, (mm/cycle) / (MPa$\sqrt{m}$ ). |
| a | Length of crack, meter. |
| $a_i$ | Last length in the crack, meter. |
| $a_o$ | Original length of the crack's length, meter. |
| z | Complex number that gives the possibility of calculating any place on the slide in the stress function |
| $\boldsymbol{\theta}$, $\boldsymbol{\theta}_1$, $\boldsymbol{\theta}_2$ | Different angles relative to the location expressed by (z) |
| r, $r_1$, $r_2$ | Radius from the different corners $\boldsymbol{\theta}$, $\boldsymbol{\theta}_1$, $\boldsymbol{\theta}_2$, to the (z) position |
| $\boldsymbol{\phi}_{Z(I+II)}$ | Stress function for mixed mode (I/II) |
| E' | Modulus of elastic, Mega Pascal. |
| v | Displacement for the mixed mode. |
| $\dot{v}$ | Rate of displacement for the mixed mode. |
| $\boldsymbol{\tau}_o$ | Max value of shear stress, Mega Pascal. |
| $\boldsymbol{\tau}$ | Shear cycling load (mode II), Mega Pascal. |
| w | Angular velocity, rad /sec. |
| t | Time, seconds. |
| mass | Mass of the material, kilogram. |
| $T_{total}$ | Total amount of kinetic energy, Joule. |
| G | Release energy rate of increase in fracture length, joule. |
| R | Amount of energy being resisted by the fracture, joule. |
| $K_I$ | Stress intensity factor for mode I, MPa$\sqrt{m}$. |
| $K_{II}$ | Stress intensity factor for mode II, MPa$\sqrt{m}$. |
| $\boldsymbol{\sigma}_{eff}$ | The effective stress for the mixed mode, Mega Pascal. |
| U | Total amount of excess energy, joule. |
| $U_O$ | The amount of excess energy per unit of thickness for edge crack, joule. |
| da /dt | Rate of crack growth, m/sec. |
| $\boldsymbol{\sigma}$ | Tension stress, Mega Pascal. |
| $\Theta_c$ | Angel of crack, degree |
| $\boldsymbol{\upsilon}$ | Poisson's ratio, unit less |
| ρ | Density of the material, kg/m$^3$ |

**Declaration of interest**

The authors declare that they have no conflicts of interest financial or personal relationships with other persons or organisations that could improperly influence their work in connection with the publication of this article.

**Submission declaration**

The authors declare that the work described has not been previously published, that it is not under consideration for publication elsewhere, and that all authors have approved its publication in connection with the publication of this article.

## Acknowledgement

We thank everyone who have helped publish this study. We also thank the Mechanical Department at Baghdad University for providing us with the resources and assistance to finish this project. Finally, we appreciate all research participants' time and willingness to share their experiences. Their contributions have been crucial to our understanding and conclusions.

**Funding sources**

This research did not receive any specific grant from funding agencies in the public, commercial, or not-for-profit sectors.

## References

[1] P. Zhang, J. Li, Y. Zhao, and J. Li, "Crack propagation analysis and fatigue life assessment of high-strength bolts based on fracture mechanics.," *Sci. Rep.*, vol. 13, no. 1, p. 14567, Sep. 2023, doi: 10.1038/s41598-023-41804-z.

[2] A. Al-Mukhtar, "Mixed-Mode Crack Propagation in Cruciform Joint using Franc2D," *J. Fail. Anal. Prev.*, vol. 16, Apr. 2016, doi: 10.1007/s11668-016-0094-1.

[3] D. Rozumek and E. Macha, "A survey of failure criteria and parameters in mixed-mode fatigue crack growth," *Mater. Sci.*, vol. 45, no. 2, p. 190, 2009, doi: 10.1007/s11003-009-9179-2.

[4] A. D. Assi, "Influence of Al2O3 Nanoparticles Addition to AA6082-T6 on Mechanical Properties by Stir Casting Technique," *IOP Conf. Ser. Mater. Sci. Eng.*, vol. 881, no. 1, p. 12081, 2020, doi: 10.1088/1757-899X/881/1/012081.

[5] F. Alshamma and O. Jassim, "Dynamic crack propagation in nano-composite thin plates under multi-axial cyclic loading," *J. Mater. Res. Technol.*, vol. 8, Aug. 2019, doi: 10.1016/j.jmrt.2019.08.011.

[6] B. Bachy, "MATHEMATICAL MODEL TO INVESTIGATE THE TEMPERATURE AND HARDNESS DISTRIBUTIONS DURING THE ANNEALING AND NORMALISING TREATMENT," *Intell. Transp. Syst. J.*, vol. 16, pp. 5683–5698, Jan. 2010.

[7] A. A. Asaad and M. A. Mussa, "An experimental and numerical investigation of heat transfer effect on cyclic fatigue of gas turbine blade," *J. Eng.*, vol. 25, no. 7 SE-Articles, pp. 61–82, Jun. 2019, doi: 10.31026/j.eng.2019.07.04.

[8] H. Jahed, A. Varvani-Farahani, M. Noban, and I. Khalaji, "An energy-based fatigue life assessment model for various metallic materials under proportional and non-proportional loading conditions," *Int. J. Fatigue*, vol. 29, no. 4, pp. 647–655, 2007, doi: https://doi.org/10.1016/j.ijfatigue.2006.07.01.

[9] S. A. Z. Dr. Fathi Alshamma, "No TitleCRACK GROWTH BEHAVIOR OF CRACKED COPPER PIPES (12200) UNDER CYCLIC TORSION LOADS," *Int. J. Eng. Technol. Sci. Innov.*, vol. 2, pp. 595–603, 2017, [Online]. Available: https://www.ijetsi.org/more2017.php?id=50

[10] F. A. Alshamma and M. H. Salman, "MODIFIED METHOD FOR STUDYING THE EFFECT OF LASER SHOT PEENING IN THIN PLATE ON DYNAMIC CRACK PROPAGATION UNDER CYCLING THERMAL EFFECT," 2020.

[11] F. Wang, Z. L. He, S. Yang, Z. G. Fu, H. Li, and J. H. Deng, "Investigation of Mixed-Mode Crack Propagation Behaviour under Impact Loading," *IOP Conf. Ser. Earth Environ. Sci.*, vol. 861, no. 4, p. 42007, 2021, doi: 10.1088/1755-1315/861/4/042007.

[12] A. K. Vasudevan and R. D. Doherty, *Aluminum Alloys--Contemporary Research and Applications: Contemporary Research and Applications*. in ISSN. Elsevier Science, 2012. [Online]. Available: https://books.google.iq/books?id=jGyAA1STaXEC

[13] R. J. Bucci, "Selecting aluminum alloys to resist failure by fracture mechanisms," *Eng. Fract. Mech.*, vol. 12, no. 3, pp. 407–441, 1979, doi: https://doi.org/10.1016/0013-7944(79)90053-5.

[14] R. Yamada, S. Ishizawa, G. Itoh, A. Kurumada, and M. Nakai, "Effects of environment on fatigue crack growth behavior of 2000 and 7000 series aluminum alloys," L. B. T.-R. A. in S. I. A.-P. of the I. C. (APCF/SIF-2014) Ye, Ed., Oxford: Woodhead Publishing, 2014, pp. 123–126. doi: https://doi.org/10.1533/9780081002254.123.

[15] M. D. Vijayakumar, V. Dhinakaran, T. Sathish, G. Muthu, and P. M. B. ram, "Experimental study of chemical composition of aluminium alloys," *Mater. Today Proc.*, vol. 37, pp. 1790–1793, 2021, doi: https://doi.org/10.1016/j.matpr.2020.07.391.

[16] H. Tada, H. A. Ernst, and P. C. Paris,

"Westergaard stress functions for displacement-prescribed crack problems—I," *Int. J. Fract.*, vol. 61, no. 1, pp. 39–53, 1993, doi: 10.1007/BF00032338.

[17] L. Ewalds, H and H. Wanhill, R, J, *FRACTURE MECHANICS*, FOURTH. LONDON: Edwrd Arnold, 1989.

[18] S. E. A. B. Abdel-Rahman A. Ragab, *Engineering Solid Mechanics*, Fist. Boca Raton: 20 December 2019, 1998. doi: https://doi.org/10.1201/9780203757307.

[19] [19] R. L. Liboff, *Kinetic Theory: Classical, Quantum, and Relativistic Descriptions*. in Graduate Texts in Contemporary Physics. Springer, New York, 2006. [Online]. Available: https://books.google.iq/books?id=iqASBwAAQBAJ

[20] J. knot, *fundamentals of fracture mechanics*, FIRST. LONDON, 1973.

[21] K. Sadananda, K. N. Solanki, and A. K. Vasudevan, "Subcritical crack growth and crack tip driving forces in relation to material resistance," vol. 35, no. 4–5, pp. 251–265, 2017, doi: doi:10.1515/corrrev-2017-0034.

[22] S. Alkan, P. Chowdhury, H. Sehitoglu, R. G. Rateick, and H. J. Maier, "Role of nanotwins on fatigue crack growth resistance – Experiments and theory," *Int. J. Fatigue*, vol. 84, pp. 28–39, 2016, doi: https://doi.org/10.1016/j.ijfatigue.2015.11.01.

[23] S. Hussein, M. Al-Shammari, A. Takhakh, and M. Al-Waily, "Effect of Heat Treatment on Mechanical and Vibration Properties for 6061 and 2024 Aluminum Alloys," *J. Mech. Eng. Res. Dev.*, vol. 43, pp. 48–66, Jan. 2020.

[24] S. Keil, *Technology and Practical Use of Strain Gages: With Particular Consideration of Stress Analysis Using Strain Gages*. Wiley, 2017. [Online]. Available: https://books.google.iq/books?id=7kozDwAAQBAJ

[25] T. Baral, *Paris' Law Parameters Estimation for Fatigue Crack Prediction of an Aluminum Alloy Plate Under Cyclic Loading*. University of Manitoba, 2022.https://books.google.iq/books?id=commzwEACAAJ

[26] D.-C. Ko, D.-H. Ko, J.-H. Kim, and J.-H. Park, "Development of a partition panel of an Al6061 sheet metal part for the improvement of formability and mechanical properties by hot forming quenching," *Adv. Mech. Eng.*, vol. 9, no. 2, p. 1687814017691213, Feb. 2017, doi: 10.1177/1687814017691213.

# دراسة معدلة لتأثير الاحمال المركبة بتسليط حمل الشد الثابت مع القص الدوري على انتشار تشققات الحواف الديناميكية في صفيحة رقيقة من الألومنيوم

**اسراء عبد الرزاق مصلح[1]* فتحي عبد الصاحب الشماع[2]**

*[1, 2] قسم هندسة الميكانيك، كلية الهندسة، جامعة بغداد، العراق*

*البريد الالكتروني : israa.mosleh2003m@coeng.uobaghdad.edu.iq

**المستخلص**

نظرا للأهمية والمخاطر المحتملة المرتبطة بحدوث الشقوق الميكانيكية في التطبيقات الهندسية الهامة، فقد أصبح من الضروري البحث عن نوع معين من انتشار الشقوق. هذه هي حالة شقوق الوضع المختلط التي تنتج عن الوضع الأول والوضع الثاني للتحميل والتي تنتشر في معظم الهياكل، ويتم عرض تلك الشقوق، بالإضافة إلى الظروف التي يمكن أن تحدث فيها، في هذه الحالة. في سياق نظرية ميكانيكا الكسر المرنة الخطية (LEFM)، تم تحقيق توليد إمكانية التحميل غير المتناسب على عينات من سبائك الألومنيوم من خلال تطبيق أحمال الشد الثابتة بالتزامن مع أحمال القص الدورية. باستخدام قانون جريفيث للوضع المختلط I/II لطاقة الشق، تم بناء معادلة نظرية لمعدل نمو الشق الديناميكي. تأخذ هذه المعادلة في الاعتبار تأثير انتشار الكراك الديناميكي. تجريبياً تم تصميم أجهزة مختبرية محلية الصنع وتعديلها لتتناسب مع طبيعة الأحمال المطبقة على عينات ذات شقوق حافة مسبقة من نوعين مختلفين من سبائك الألومنيوم ( (AA 6061 و5052، بنظام Uni-Standard بطول شق الحافة تم إجراء مقارنة بين أنواع السبائك المستخدمة للتحقق من صحة النتائج. والتناقض بين مدى قرب النتائج النظرية من النتائج الحقيقية للكسر الذي حدث. وأظهرت النتائج التوافق بين المعادلة النظرية والنتائج العملية. تبدأ العينة 5052 بشكل أسرع وتنتشر الشقوق بشكل أسرع من السبائك 6061.